

**NASA TECHNICAL  
MEMORANDUM**



**NASA TM X-1151**

**NASA TM X-1151**

GPO PRICE \$ \_\_\_\_\_

CSFTI PRICE(S) \$ 4.00

Hard copy (HC) \_\_\_\_\_

Microfiche (MF) 1

ff 653 July 65

**LATERAL DIRECTIONAL STABILITY  
CHARACTERISTICS AT MACH 2.3  
TO 3.5 OF A SUPERSONIC  
TRANSPORT MODEL WITH VARIOUS  
OUTBOARD VERTICAL-TAIL LOCATIONS**

*by William A. Corlett*

*Langley Research Center*

*Langley Station, Hampton, Va.*

FACILITY FORM 602

**N 65-35404**

(ACCESSION NUMBER)

351  
(PAGES)

TMX 1151  
(NASA CR OR TMX OR AD NUMBER)

(THRU)

(CODE)

C1  
(CATEGORY)

**NATIONAL AERONAUTICS AND SPACE ADMINISTRATION • WASHINGTON, D. C. • OCTOBER 1965**

LATERAL DIRECTIONAL STABILITY CHARACTERISTICS  
AT MACH 2.3 TO 3.5 OF A SUPERSONIC TRANSPORT MODEL  
WITH VARIOUS OUTBOARD VERTICAL-TAIL LOCATIONS

By William A. Corlett

Langley Research Center  
Langley Station, Hampton, Va.

NATIONAL AERONAUTICS AND SPACE ADMINISTRATION

---

For sale by the Clearinghouse for Federal Scientific and Technical Information  
Springfield, Virginia 22151 - Price \$2.00

LATERAL DIRECTIONAL STABILITY CHARACTERISTICS  
AT MACH 2.3 TO 3.5 OF A SUPERSONIC TRANSPORT MODEL  
WITH VARIOUS OUTBOARD VERTICAL-TAIL LOCATIONS

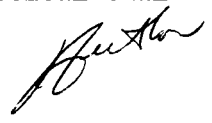
By William A. Corlett  
Langley Research Center

SUMMARY

35404

An investigation of a configuration with a highly swept blended wing-body and outboard tail surfaces has been conducted at Mach numbers from 2.3 to 3.5 to determine the effect of vertical-tail area above and below the wing-chord plane on the lateral directional stability characteristics of a transport model.

The results indicated that at low to moderate angles of attack the model with all the vertical-tail area above the wing-chord plane generally provided the highest directional-stability level, although at high supersonic Mach numbers, particularly at high angles of attack, the vertical tail surfaces below the wing-chord plane tended to become more favorable. Wing-mounted nacelles, however, detracted from the effectiveness of the lower tail surfaces. Canting the tail surfaces of the amount used for these tests had an effect on the directional stability only when applied to the lower tail surfaces. For this condition, toe-out led to increases in directional stability whereas toe-in led to decreases in directional stability. Locating the vertical tail surfaces below the wing-chord plane produced only a small reduction in effective dihedral; but, because of the accompanying decrease in the directional-stability parameter, the ratio of the directional-stability parameter to the effective-dihedral parameter was greater for the configuration with the vertical tail surfaces in the uppermost position.



INTRODUCTION

The National Aeronautics and Space Administration has conducted a number of experimental investigations directed toward the development of an aerodynamically efficient supersonic commercial-air-transport (SCAT) configuration. These studies have included wind-tunnel tests of numerous designs incorporating highly swept fixed wings and variable-sweep wings. The results of some of the more promising configurations, presented in references 1 to 4, indicate some

deterioration in directional stability with increase in angle of attack, and relatively high values of effective dihedral in the supersonic speed region that might lead to lateral directional-stability problems.

An investigation was therefore conducted to determine if changes in vertical-tail area above and below the wing-chord plane could alleviate these adverse lateral directional stability characteristics. Additional tests were performed on the model of reference 4 (SCAT 15-2.6), which is a configuration with a highly swept blended wing-body and outboard tail surfaces. The results of these tests are presented herein. This study was made in the Langley Unitary Plan wind tunnel at Mach numbers from 2.3 to 3.5, at angles of attack from  $-4^\circ$  to  $13^\circ$ , and at sideslip angles of  $0^\circ$  and  $4^\circ$ . The tests were performed at a Reynolds number of  $3.26 \times 10^6$ , based on the mean aerodynamic chord.

## SYMBOLS

All data are referenced to the body-axis system. The moment reference point is at a longitudinal station corresponding to 75.9 percent of the body length. The units for the physical quantities in this paper are given both in U.S. Customary Units and in the International System of Units (SI). (See ref. 5.)

The coefficients and symbols are defined as follows:

b reference wing span excluding horizontal tip tails, 16.00 in.  
(40.64 cm)

$C_l$  rolling-moment coefficient,  $\frac{\text{Rolling moment}}{qSb}$

$C_n$  yawing-moment coefficient,  $\frac{\text{Yawing moment}}{qSb}$

$C_y$  side-force coefficient,  $\frac{\text{Side force}}{qS}$

$C_{l\beta}$  effective-dihedral parameter,  $\left(\frac{\Delta C_l}{\Delta \beta}\right)_{\beta=0^\circ, 4^\circ}$

$C_{n\beta}$  directional-stability parameter,  $\left(\frac{\Delta C_n}{\Delta \beta}\right)_{\beta=0^\circ, 4^\circ}$

$C_{y\beta}$  side-force parameter,  $\left(\frac{\Delta C_y}{\Delta \beta}\right)_{\beta=0^\circ, 4^\circ}$

$\Delta C_{l\beta,t}$  vertical-tail contribution to  $C_{l\beta}$

$\Delta C_{n\beta,t}$	vertical-tail contribution to $C_{n\beta}$
$\Delta C_{Y\beta,t}$	vertical-tail contribution to $C_{Y\beta}$
M	free-stream Mach number
$p_t$	stagnation pressure, lbf/sq ft ( $N/m^2$ )
q	free-stream dynamic pressure, lbf/sq in. ( $N/m^2$ )
S	reference wing area including fuselage intercept but excluding horizontal tail, 219.46 sq in. (1416 sq cm)
$T_t$	stagnation temperature, $^{\circ}F$ ( $^{\circ}R$ )
$\alpha$	angle of attack, deg
$\beta$	angle of sideslip, deg
$\delta_h$	horizontal-tail deflection, deg
$\phi$	vertical-tail cant angle, deg (positive for toe-out)

Model component designations:

W	wing
B	body
E	engine nacelle
H	horizontal tail
$V_1$	vertical-tail surface in uppermost position for which vertical-tail area is above wing-chord plane
$V_2$	vertical-tail surface for which one-third of vertical-tail area is transferred below wing-chord plane
$V_3$	vertical-tail surface for which two-thirds of vertical-tail area is transferred below wing-chord plane
$V_4$	vertical-tail surface for which all vertical-tail area is transferred below wing-chord plane

## MODEL AND APPARATUS

Dimensional details of the model are shown in figures 1 and 2, with additional geometric characteristics presented in table I. The basic model was the same as for reference 4, except for the vertical tails which in this investigation had about 50 percent greater area. In addition to the basic vertical tails, three other sets of vertical tails were constructed so that the area above the wing-chord plane was removed in three equal increments and placed below the wing-chord plane in such a manner as to maintain a constant vertical-tail area. The vertical tails could also be canted from the original  $-2^\circ$  (toe-in position), to  $0^\circ$ , and to  $2^\circ$  (toe-out position) by installing wedges between the tail surfaces and mountings.

The tests were conducted in the high Mach number test section of the Langley Unitary Plan wind tunnel, which is a variable-pressure continuous-flow facility. The nozzle leading to the test section is of the asymmetric sliding-block type which permits a continuous variation in test-section Mach number from about 2.3 to 4.7.

Aerodynamic forces and moments on the model were measured by means of an internally mounted, electrical, strain-gage balance. The balance was attached to a sting which, in turn, was rigidly fastened to the tunnel support system.

## TESTS, CORRECTIONS, AND ACCURACY

For all tests the Reynolds number was  $3.26 \times 10^6$  based on the mean aerodynamic chord. The stagnation dewpoint was maintained below  $-30^\circ \text{ F}$  ( $239^\circ \text{ K}$ ) to prevent condensation effects. The stagnation temperature was  $150^\circ \text{ F}$  ( $339^\circ \text{ K}$ ). The stagnation pressure varied as follows for the test Mach numbers:

M	$P_t$	
	lbf/sq ft	kN/m <sup>2</sup>
2.30	1914	91.64
2.60	2234	106.96
2.96	2704	129.47
3.50	3600	172.37

The angle of attack was varied from about  $-4^\circ$  to  $13^\circ$  at angles of sideslip of about  $0^\circ$  and  $4^\circ$ . The angles of attack and sideslip have been corrected for the deflection of the sting and balance due to aerodynamic forces on the model. Angles of attack have also been corrected for tunnel-flow angularity. In order to assure a turbulent boundary layer, 1/16-inch-wide (0.159-centimeter-wide) strips of No. 80 carborundum grit were placed on the wing and tail surfaces 1/8 inch (0.318 cm) from the leading edge (measured normal to the leading edge),

and a 1/16-inch-wide (0.159-centimeter-wide) strip of No. 60 carborundum grit was placed 1/2 inch (1.270 cm) behind and around the model nose. Transition strips were also placed on the engine nacelles 1/2 inch (1.270 cm) behind the lip; No. 120 carborundum grit was used internally and No. 80 carborundum grit was used externally.

Based on balance calibration and repeatability of the data, it is estimated that the various measured quantities are accurate within the following limits:

$C_l$ . . . . .	$\pm 0.0002$
$C_n$ . . . . .	$\pm 0.0008$
$C_y$ . . . . .	$\pm 0.005$
$\alpha$ , deg . . . . .	$\pm 0.1$
$\beta$ , deg . . . . .	$\pm 0.1$
$M$ . . . . .	$\pm 0.015$

## RESULTS AND DISCUSSION

The effect of the amount of vertical-tail area above or below the wing-chord plane on the lateral aerodynamic parameters of the model is shown in figure 3. The greatest directional stability for the model is generally obtained with all the vertical-tail area above the wing-chord plane ( $V_1$ ) in the angle-of-attack and Mach number range of these tests. Decreasing the vertical-tail area above the wing-chord plane leads to a decrease in  $C_{n\beta}$ , particularly at angles of attack near  $0^\circ$ . This decrease in  $C_{n\beta}$  is apparently related to the wing camber and twist, which probably induces a region of separated flow beneath the wing tip at low angles of attack causing a decrease in the increments of  $C_{y\beta}$  and  $C_{n\beta}$  for the tail surfaces in the lower positions. With increasing angle of attack it would be expected that the effectiveness of the lower tails would initially increase as the separated region diminishes. Only at the highest test Mach number and angle of attack (fig. 3(d)) does the effectiveness of the lowest tail ( $V_4$ ) begin to exceed that of the uppermost tail ( $V_1$ ) because of the high pressure field generated on the underside of the wing at positive angles of attack and particularly at the higher supersonic Mach numbers.

As expected, less negative values of  $C_{l\beta}$  are obtained for the model with tail  $V_4$ . However, the reduction in effective dihedral ( $-C_{l\beta}$ ) between the  $V_1$  and  $V_4$  tails is only from about 0.0003 to 0.0005 in the Mach number and angle-of-attack range for the configurations with the engines on. Because of the accompanying decrease in  $C_{n\beta}$ , the ratio of  $C_{n\beta}$  to  $C_{l\beta}$  is still greater for the upper-surface tails ( $V_1$ ) than for the lower-surface tails ( $V_4$ ).

There appears to be no significant effect of canting the  $V_1$  tails  $-2^\circ$  (toe-in) on the lateral directional parameters of the model throughout the

angle-of-attack and Mach number range (fig. 4). With the vertical tails in the lowest position (see fig. 5), canting the  $V_4$  tails  $-2^\circ$  (toe-in) gives a decrease in  $C_{n\beta}$ ; whereas, canting the tails  $2^\circ$  (toe-out) provides an increase in  $C_{n\beta}$  at all test Mach numbers and angles of attack. These data also indicate that the effects of toe-in or toe-out on  $C_{n\beta}$  are accentuated with increase in angle of attack, particularly at the higher Mach numbers. There appears to be little or no effect of toe-in or toe-out of the  $V_4$  tails on the effective dihedral of the model.

The effectiveness of the  $V_1$  and  $V_4$  tails in producing directional stability and effective dihedral with and without the engine nacelles is shown in figure 6 and summarized in figure 7. The directional stability of both the  $V_1$  and  $V_4$  model configurations is greater with the nacelles on than with the nacelles off at positive angles of attack. Also, the values of  $C_{l\beta}$  for the nacelle-on configurations are more negative. (See fig. 6.) The tail-contribution data presented in figure 7, however, show that the effectiveness of the  $V_1$  tails in producing directional stability is essentially unaffected by the nacelles, whereas, the nacelles greatly reduce the effectiveness of the  $V_4$  tails in producing  $C_{n\beta}$ . The effectiveness of either set of vertical tails ( $V_1$  or  $V_4$ ) in producing effective dihedral is essentially unaffected by the nacelles.

#### CONCLUSIONS

Tests of a configuration with a highly swept blended wing-body and outboard tail surfaces have been performed at Mach numbers from 2.3 to 3.5 to determine the effect of vertical-tail area above and below the wing-chord plane on the lateral directional stability characteristics. The results of these tests indicated the following conclusions:

1. The configuration (nacelles on) having all the vertical-tail area above the wing-chord plane provided the highest directional-stability level except at the highest Mach number and at the high angles of attack where the vertical-tail surface below the wing-chord plane tended to become more favorable.

2. The presence of the engine nacelles had little effect on the uppermost tail surfaces but reduced the effectiveness of the lowest tail surfaces.

3. Canting the tail surfaces of the amount used for these tests had little effect on directional stability when applied to the vertical tail surfaces in the uppermost position; whereas, for the tails in the lowest position, toe-out caused an increase in directional stability and toe-in caused a decrease in directional stability.

4. Locating the vertical tail surfaces below the wing-chord plane produced only a small reduction in effective dihedral; and, because of the accompanying



decrease in the directional-stability parameter, the ratio of the directional-stability parameter to the effective-dihedral parameter was greater for the uppermost tail-surface configuration.

Langley Research Center,  
National Aeronautics and Space Administration,  
Langley Station, Hampton, Va., July 15, 1965.

#### REFERENCES

1. Whitcomb, Richard T.; Patterson, James C., Jr.; and Kelly, Thomas C.: An Investigation of the Subsonic, Transonic, and Supersonic Aerodynamic Characteristics of a Proposed Arrow-Wing Transport Airplane Configuration. NASA TM X-800, 1963.
2. Fuller, Dennis E.; and Weirich, Robert L.: Aerodynamic Characteristics at Mach Numbers From 0.50 to 2.96 of a Supersonic Transport Model With a Variable-Sweep High-Panel-Aspect-Ratio Wing. NASA TM X-980, 1964.
3. Robins, A. Warner; Spearman, M. Leroy; and Harris, Roy V., Jr.: Aerodynamic Characteristics at Mach Numbers of 2.30, 2.60, and 2.96 of a Supersonic Transport Model With a Blended Wing-Body, Variable-Sweep Auxiliary Wing Panels, Outboard Tail Surfaces, and a Design Mach Number of 2.6. NASA TM X-815, 1963.
4. Harris, Roy V., Jr.; and Corlett, William A.: Transonic Aerodynamic Characteristics of a Supersonic Transport Model With Variable-Sweep Auxiliary Wing Panels, Outboard Tail Surfaces and a Design Mach Number of 2.6. NASA TM X-1075, 1965.
5. Mechtly, E. A.: The International System of Units - Physical Constants and Conversion Factors. NASA SP-7012, 1964.

TABLE I.- GEOMETRIC CHARACTERISTICS OF THE MODEL

## Wing:

Sweep angle of leading edge, deg . . . . .	75
Sweep angle of trailing edge, deg . . . . .	56.18
Aspect ratio . . . . .	1.166
Span, in. (cm) . . . . .	16.0 (40.64)
Reference area, sq in. (sq cm) . . . . .	219.46 (1416)
Root chord, in. (cm) . . . . .	22.67 (57.58)
Tip chord (including auxiliary wing panel at $\Lambda = 75^\circ$ ), in. (cm) . . . . .	4.76 (12.09)
Mean aerodynamic chord, in. (cm) . . . . .	15.67 (39.80)

## Fuselage:

Length, in. (cm) . . . . .	40.84 (103.73)
Balance-chamber area, sq in. (sq cm) . . . . .	2.68 (17.29)

## Horizontal tail:

Area (both), sq in. (sq cm) . . . . .	16.57 (106.8)
Thickness ratio . . . . .	0.03
Airfoil section . . . . .	Circular arc

## Vertical tail:

Area (both), sq in. (sq cm) . . . . .	28.74 (185.4)
Thickness ratio . . . . .	0.02
Airfoil section . . . . .	Half circular arc

## Nacelles:

Length, in. (cm) . . . . .	7.500 (19.05)
Base area (each), sq in. (sq cm) . . . . .	0.749 (4.83)
Inboard nacelle location -	
Cant angle, deg . . . . .	0.75
Longitudinal distance from model nose to lip of nacelle, in. (cm) . . . . .	32.6 (82.80)
Lateral distance from model reference line to center line of nacelle at inlet, in. (cm) . . . . .	2.500 (6.35)
Vertical distance from model reference line to nacelle center line, in. (cm) . . . . .	0.937 (2.38)
Outboard nacelle location -	
Cant angle, deg . . . . .	1.5
Longitudinal distance from model nose to lip of nacelle, in. (cm) . . . . .	38.1 (96.77)
Lateral distance from model reference line to center line of nacelle at inlet, in. (cm) . . . . .	5.000 (12.70)
Vertical distance from model reference line to nacelle center line, in. (cm) . . . . .	0.462 (1.17)

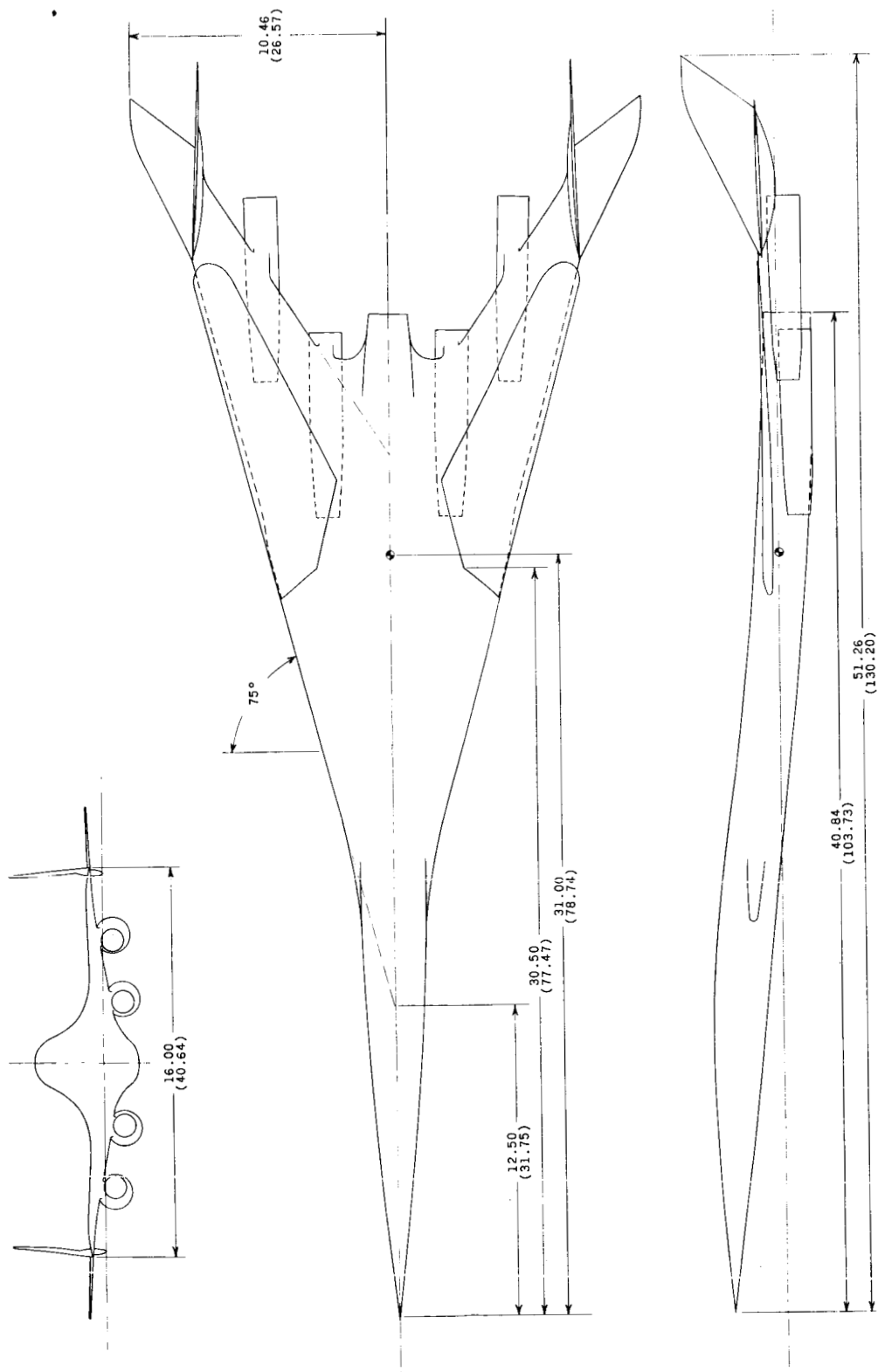


Figure 1.- Model details. (All dimensions are given in inches and parenthetically in centimeters.)

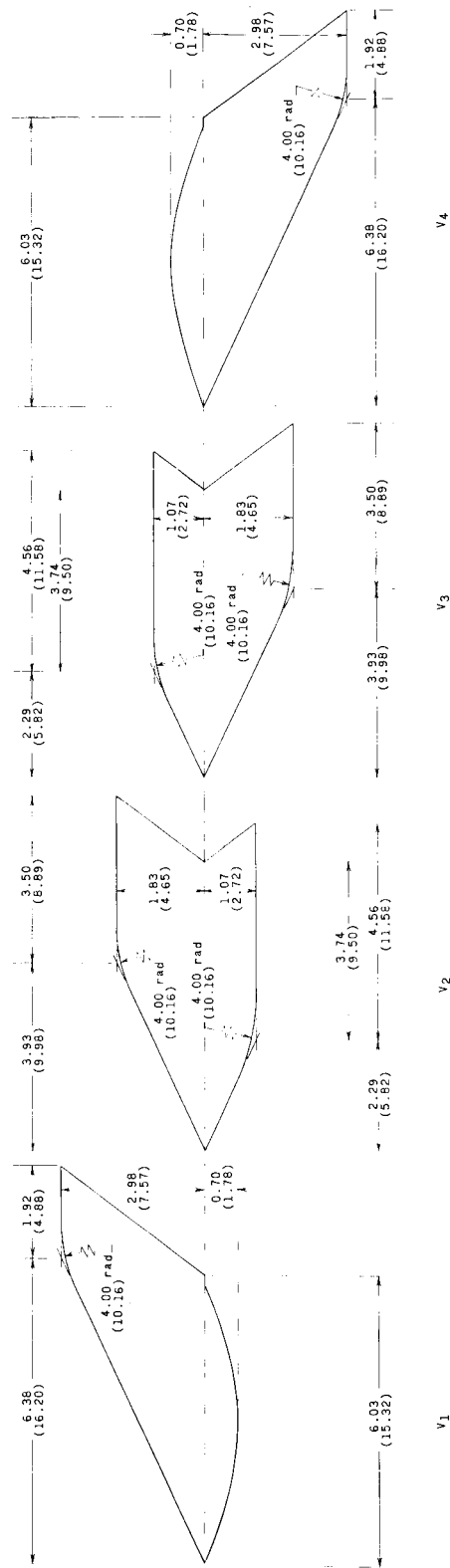
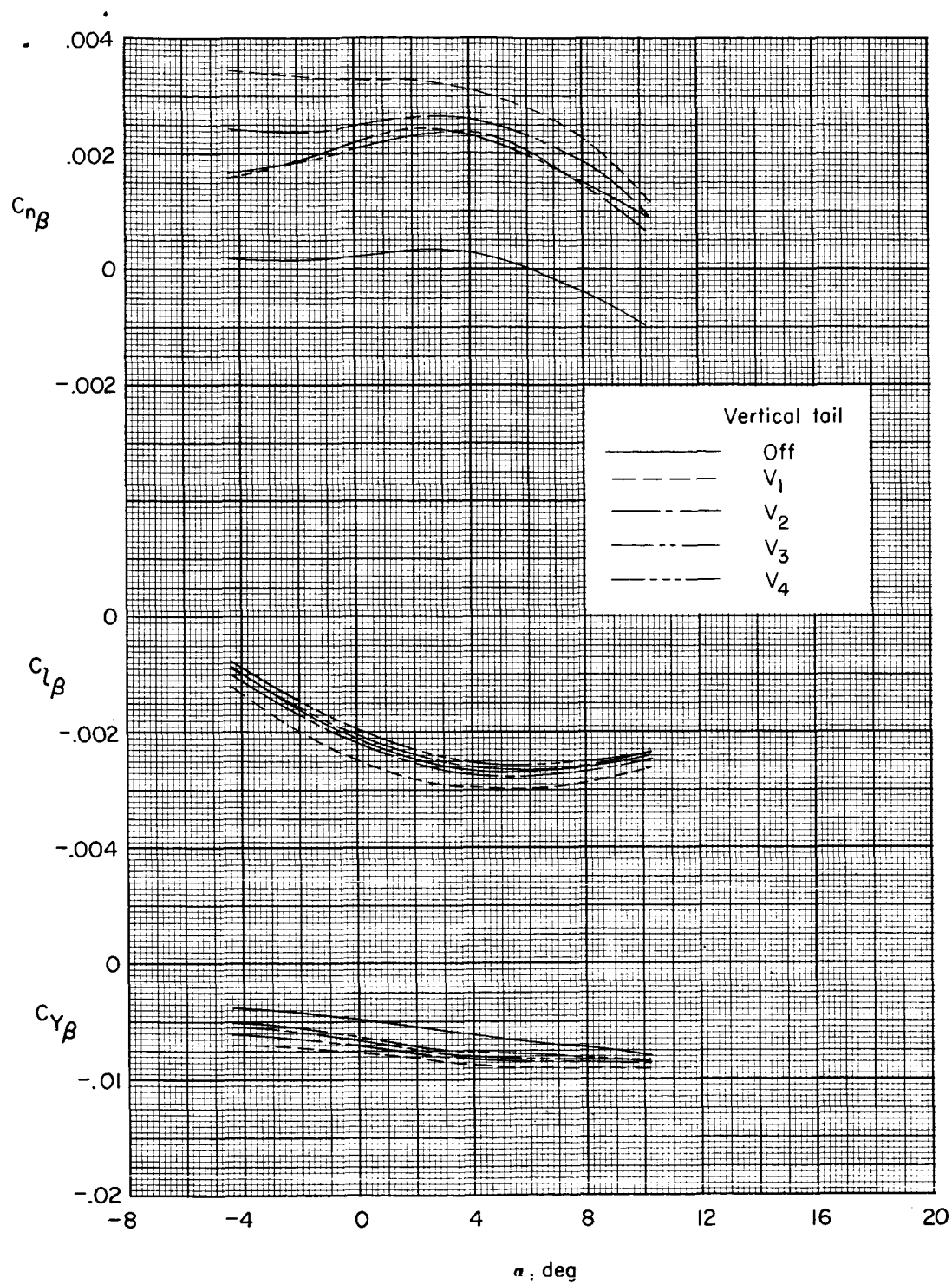
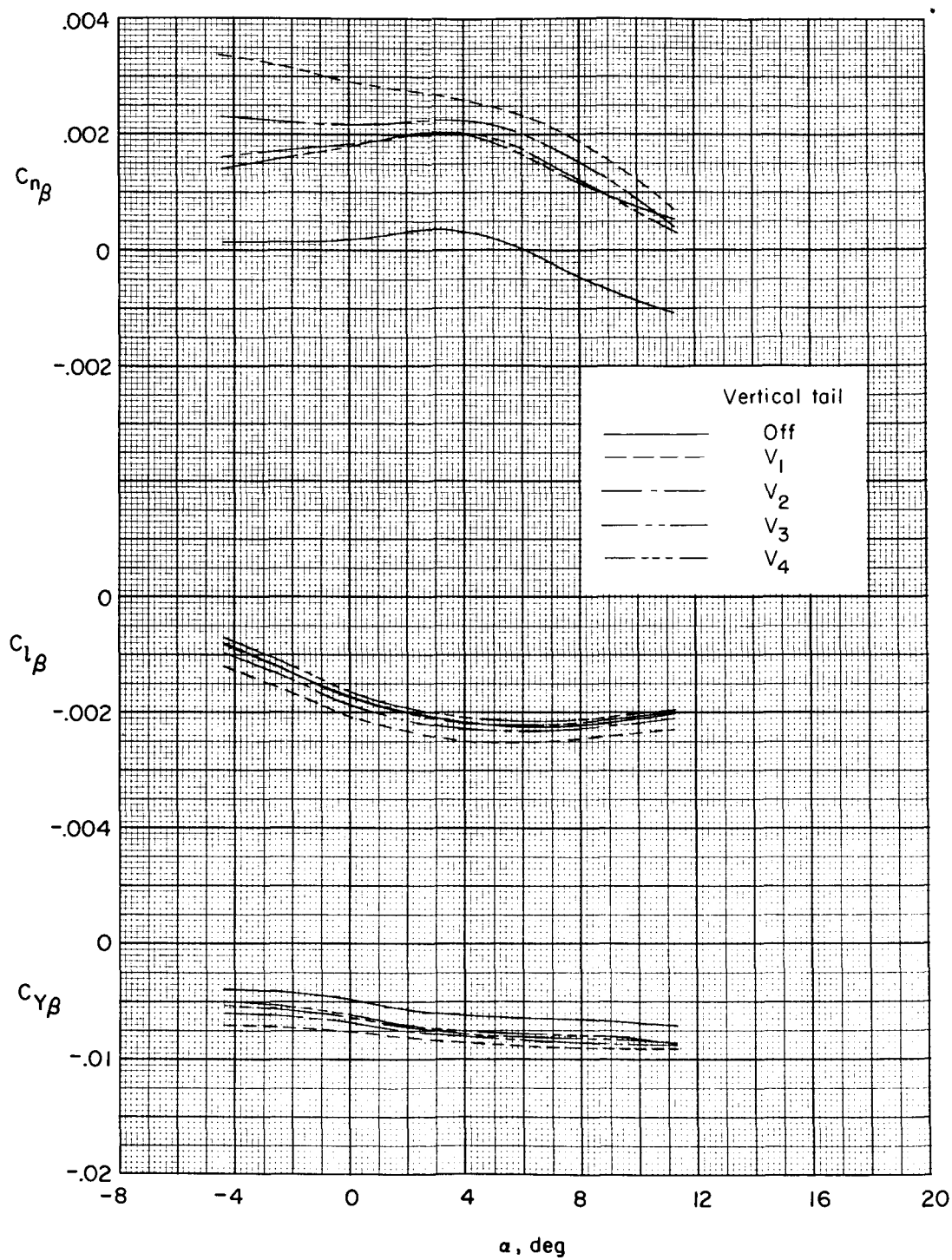


Figure 2.- Details of various vertical-tail surfaces. (All dimensions are given in inches and parenthetically in centimeters.)



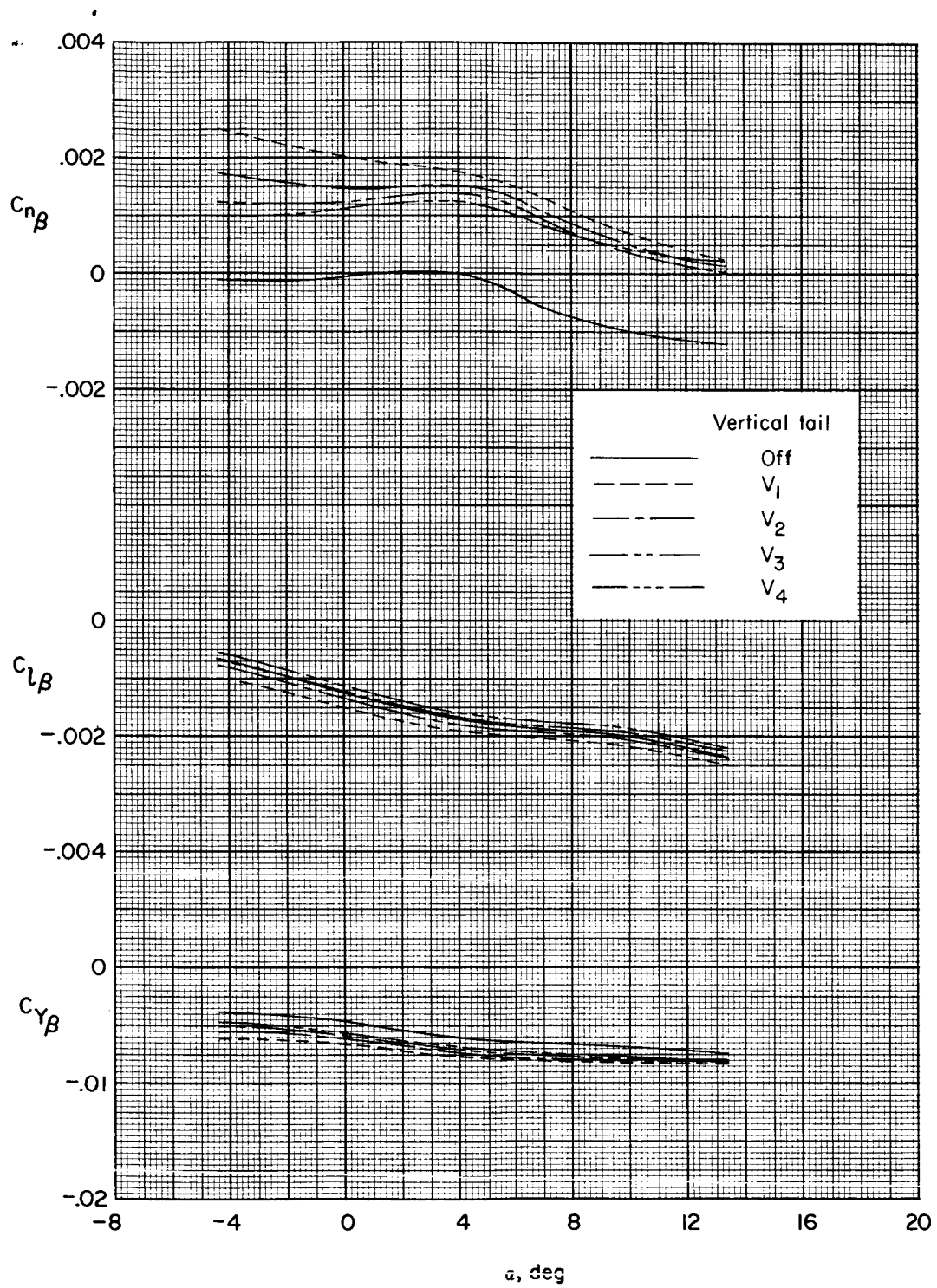
(a)  $M = 2.30$ .

Figure 3.- Effect of vertical-tail location on lateral directional-stability parameters. Engine nacelles on;  $\delta_h = -2^\circ$ ;  $\phi = 2^\circ$ .



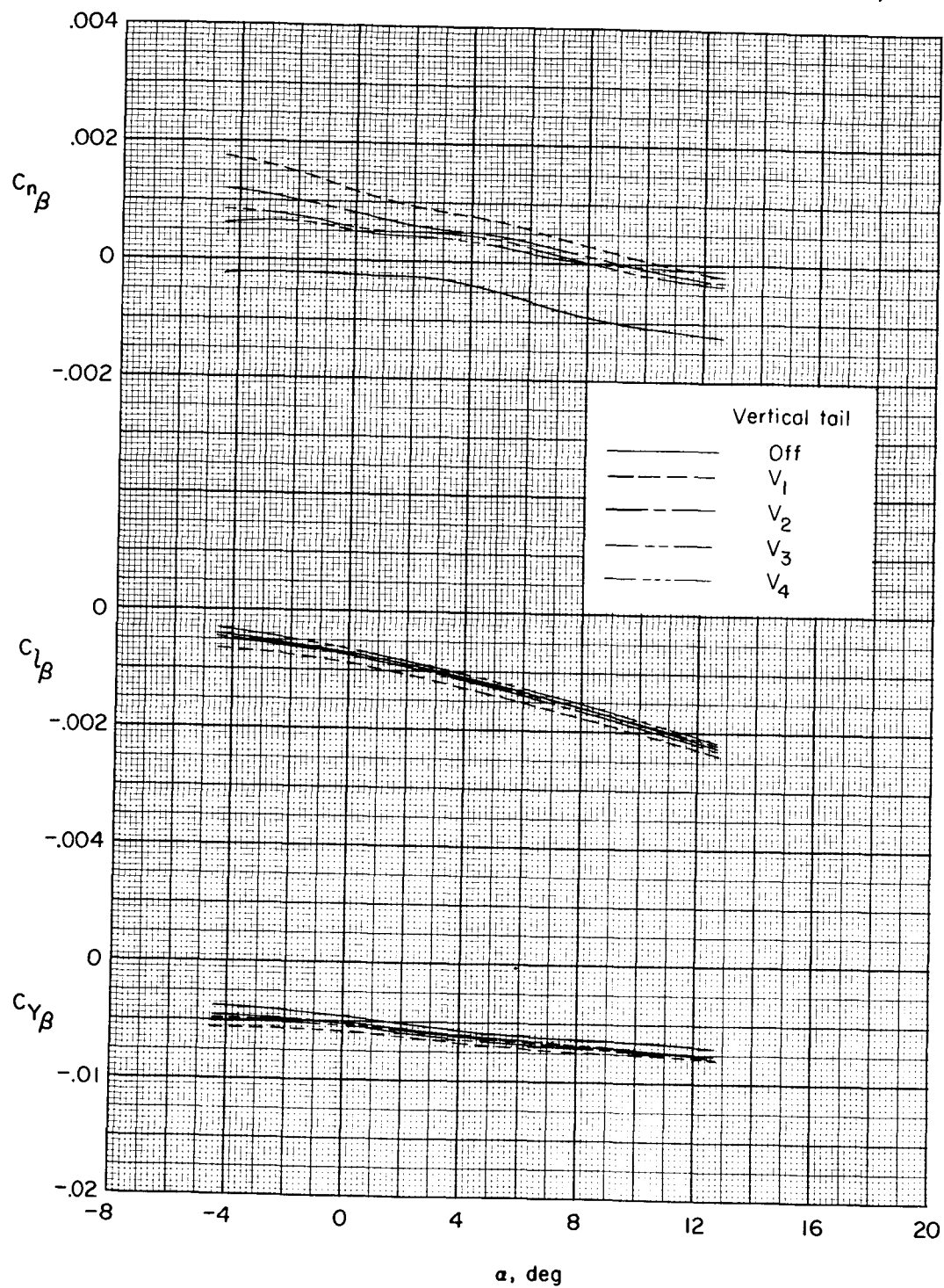
(b)  $M = 2.60$ .

Figure 3.- Continued.



(c)  $M = 2.96$ .

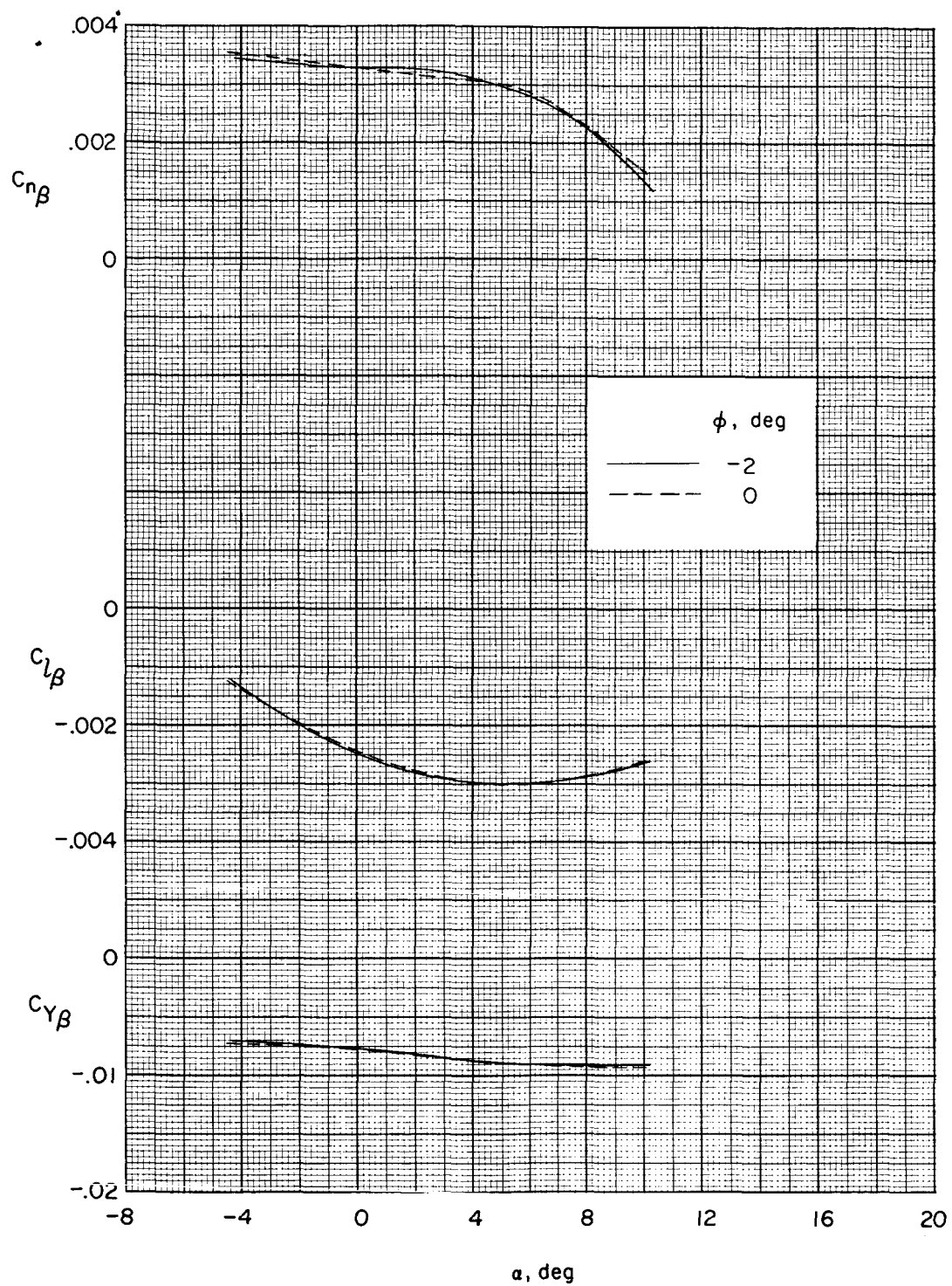
Figure 3.- Continued.



(d)  $M = 3.50$ .

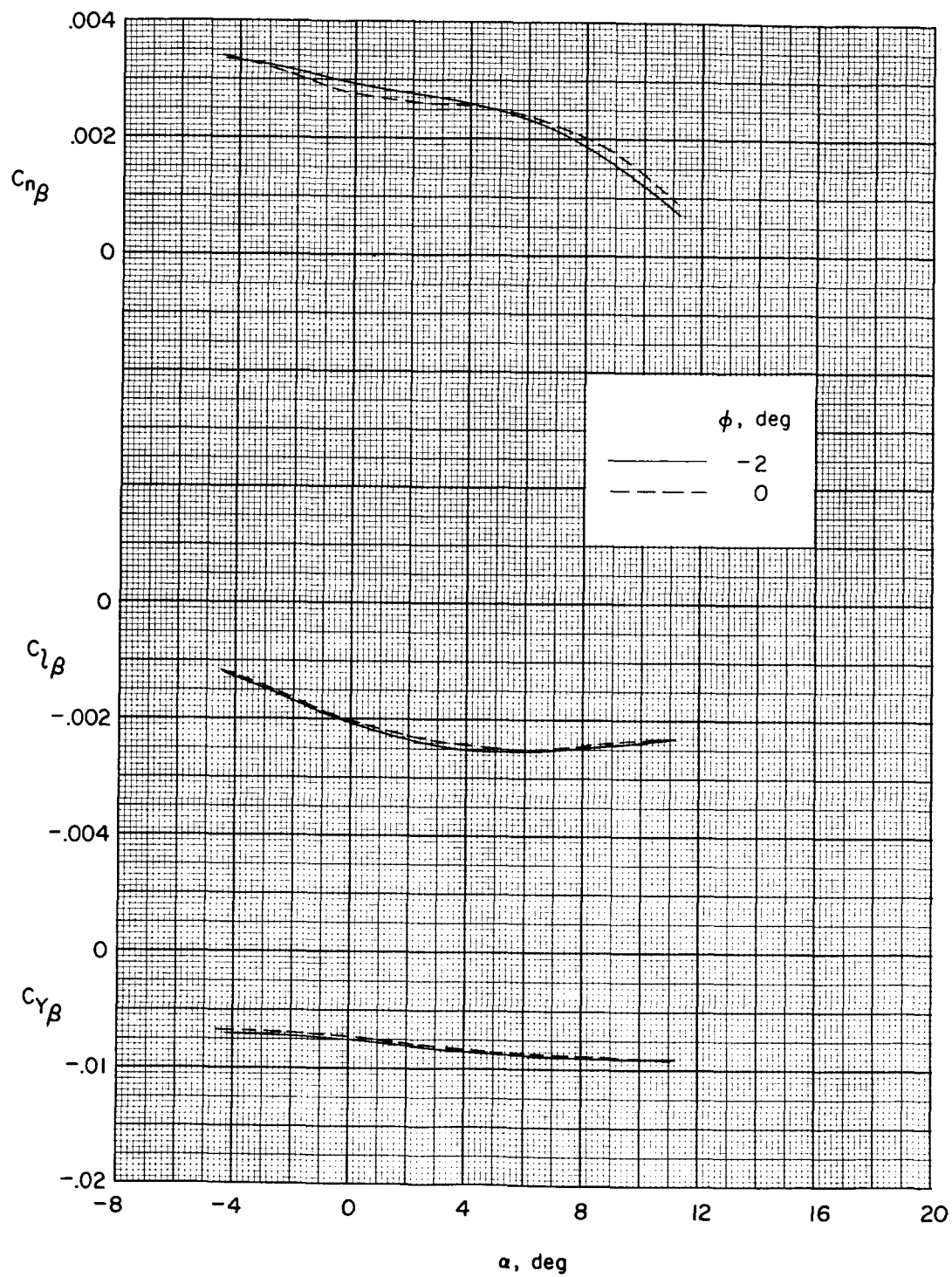
Figure 3.- Concluded.





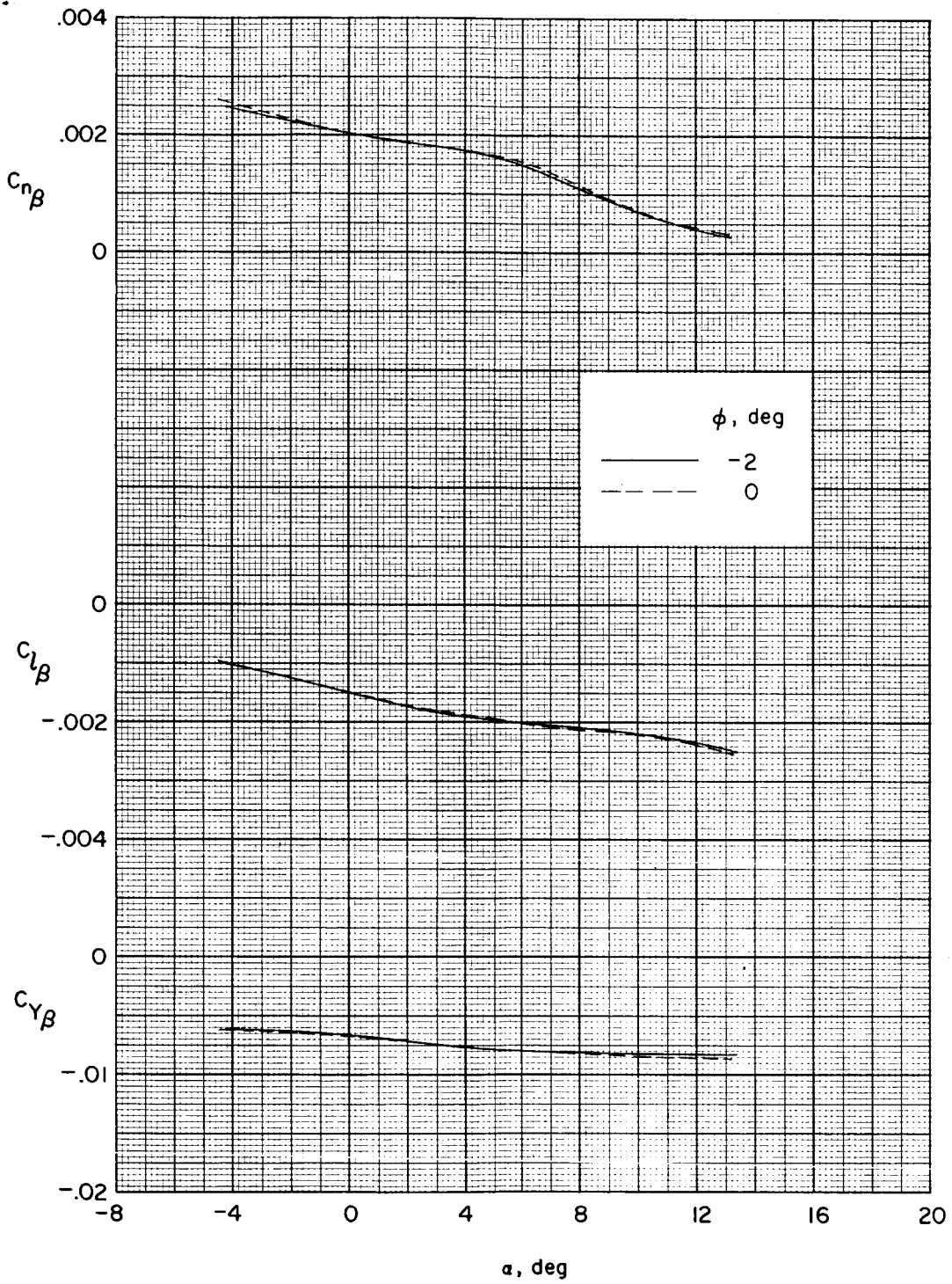
(a)  $M = 2.30$ .

Figure 4.- Effect of cant angle on lateral directional-stability parameters for model with  $V_1$  tails. Engine nacelle on;  $\delta_h = -2^\circ$ .



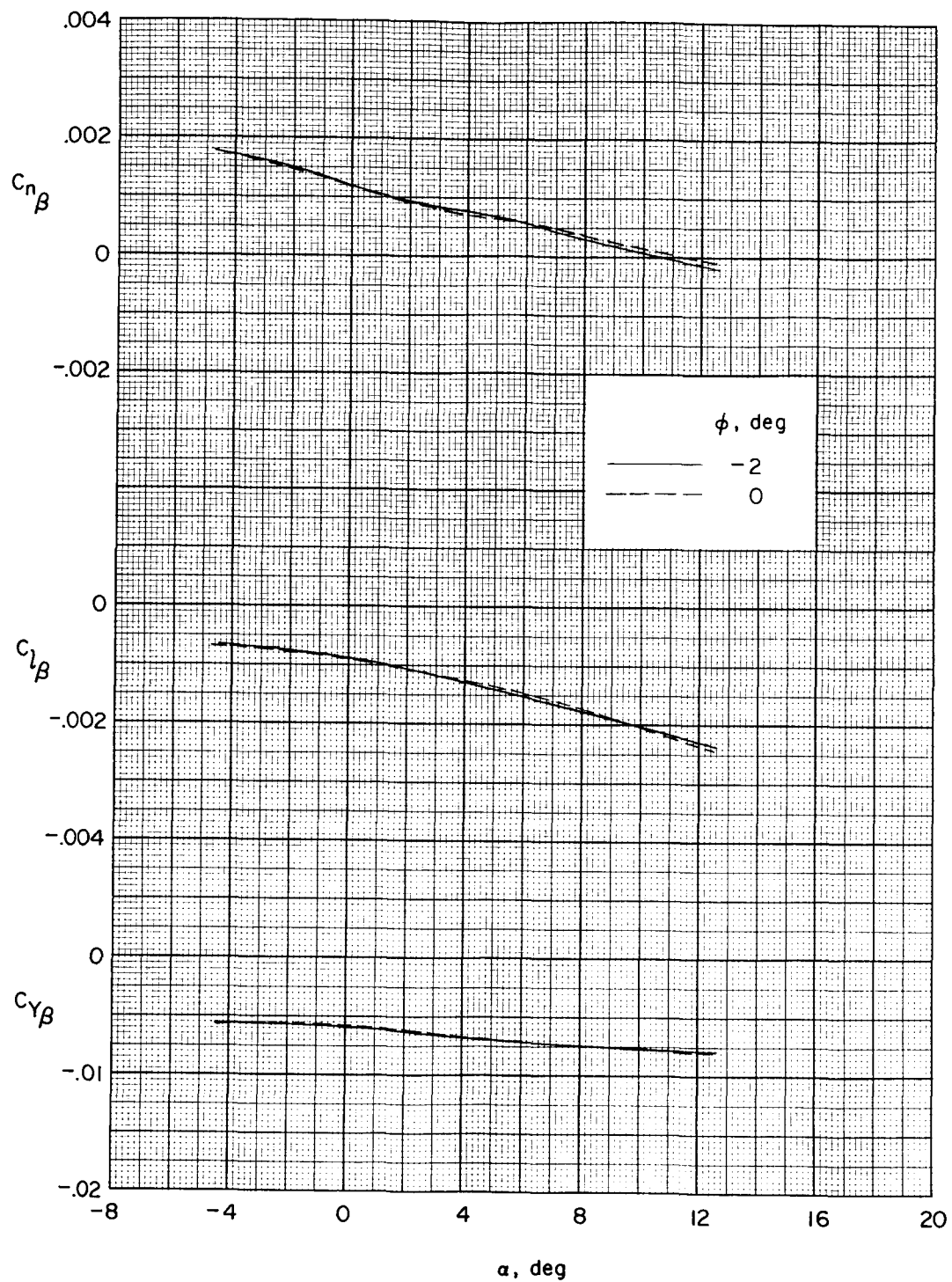
(b)  $M = 2.60$ .

Figure 4.- Continued.



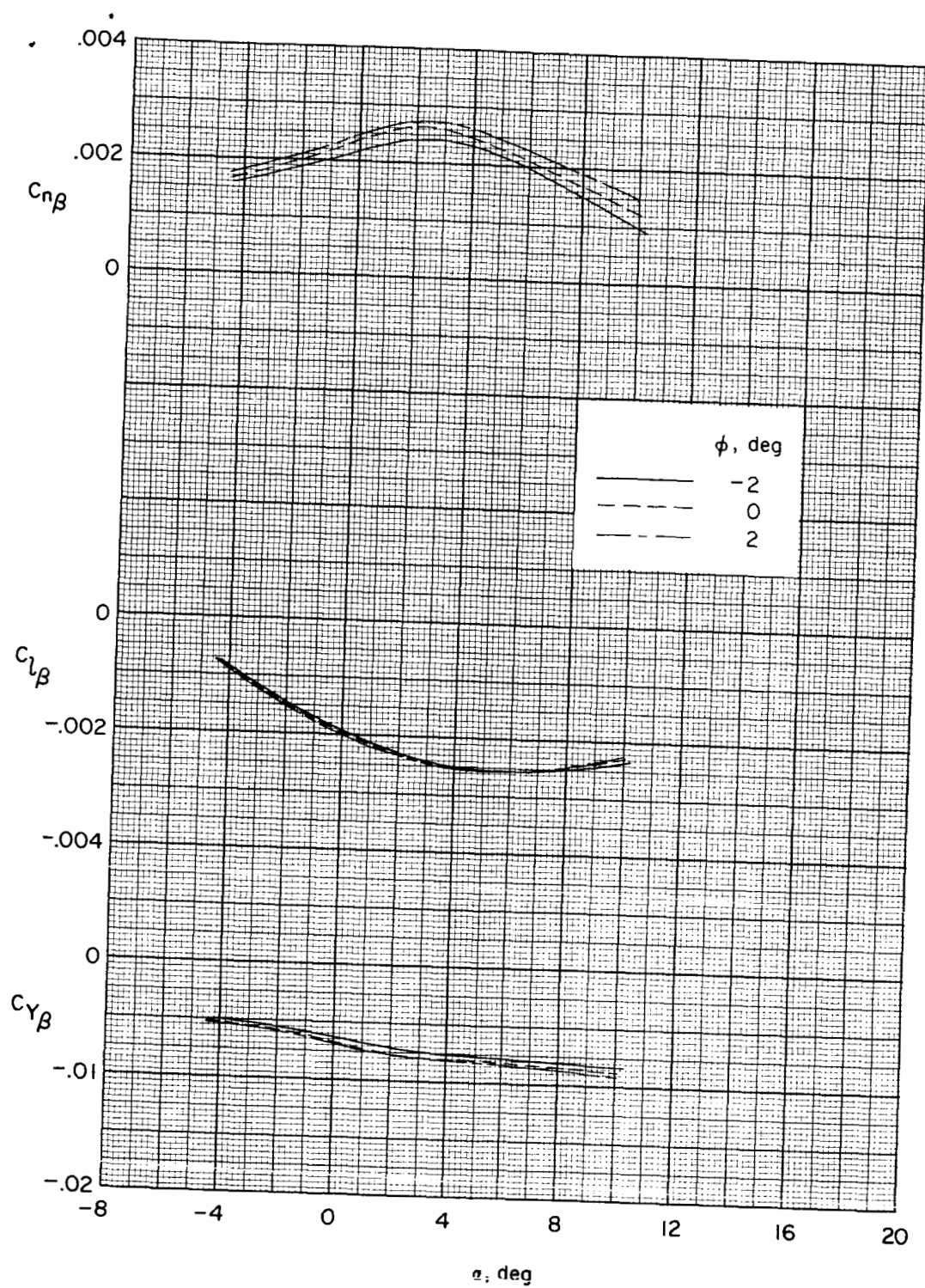
(c)  $M = 2.96$ .

Figure 4.- Continued.



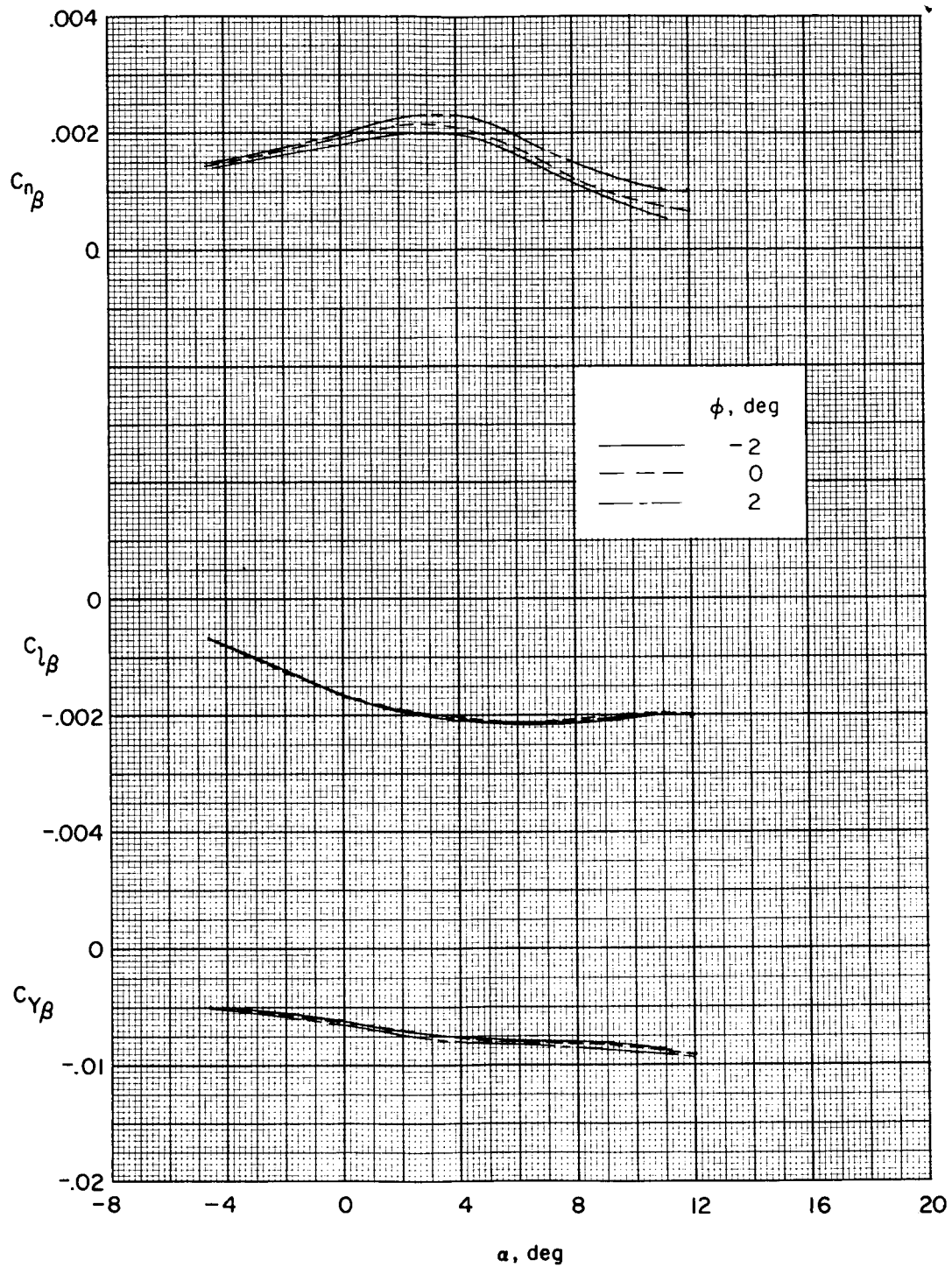
(d)  $M = 3.50$ .

Figure 4.- Concluded.



(a)  $M = 2.30$ .

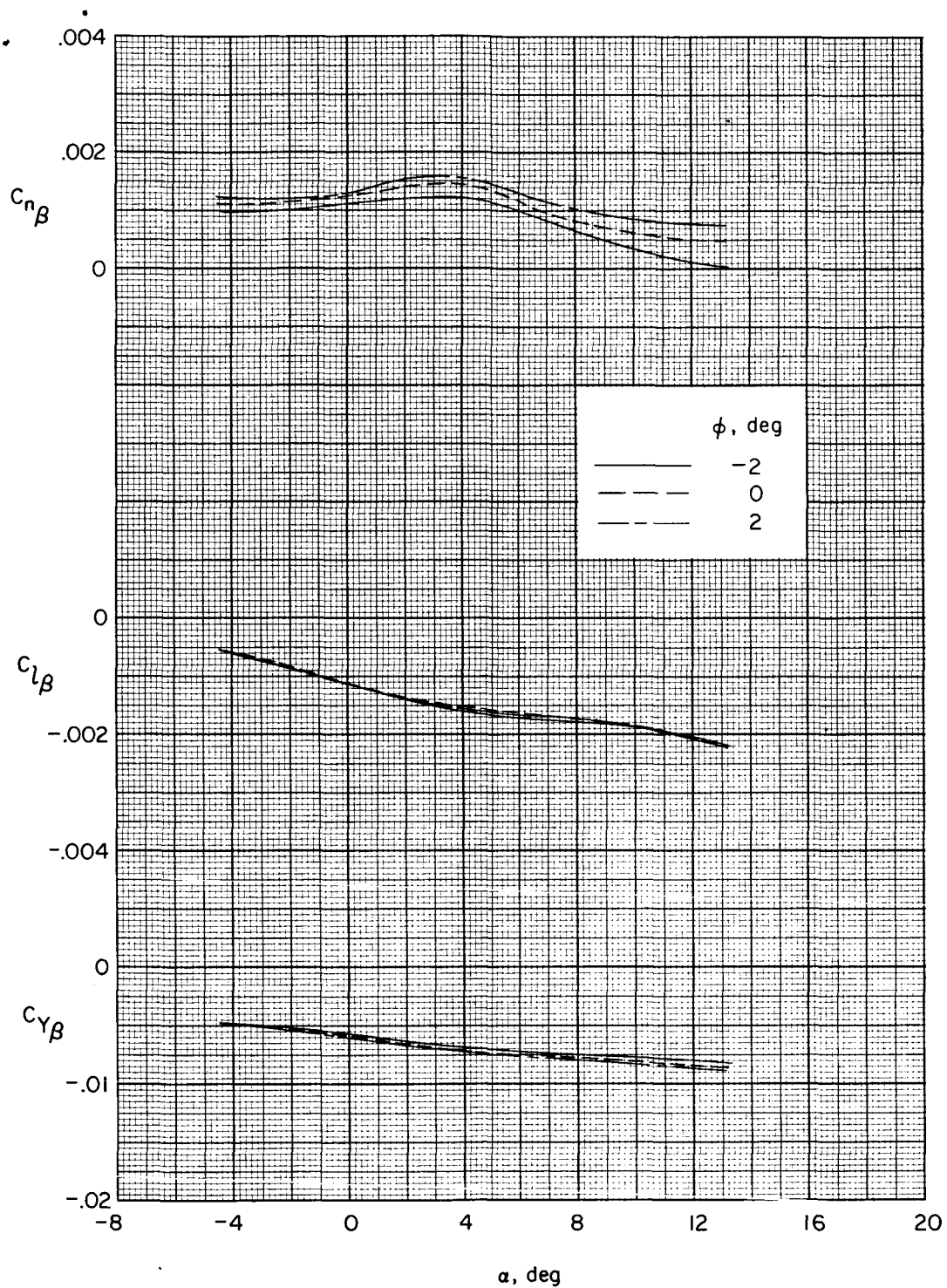
Figure 5.- Effect of cant angle on lateral directional-stability parameters for model with  $V_4$  tails. Engine nacelles on;  $\delta_H = -2^\circ$ .



(b)  $M = 2.60$ .

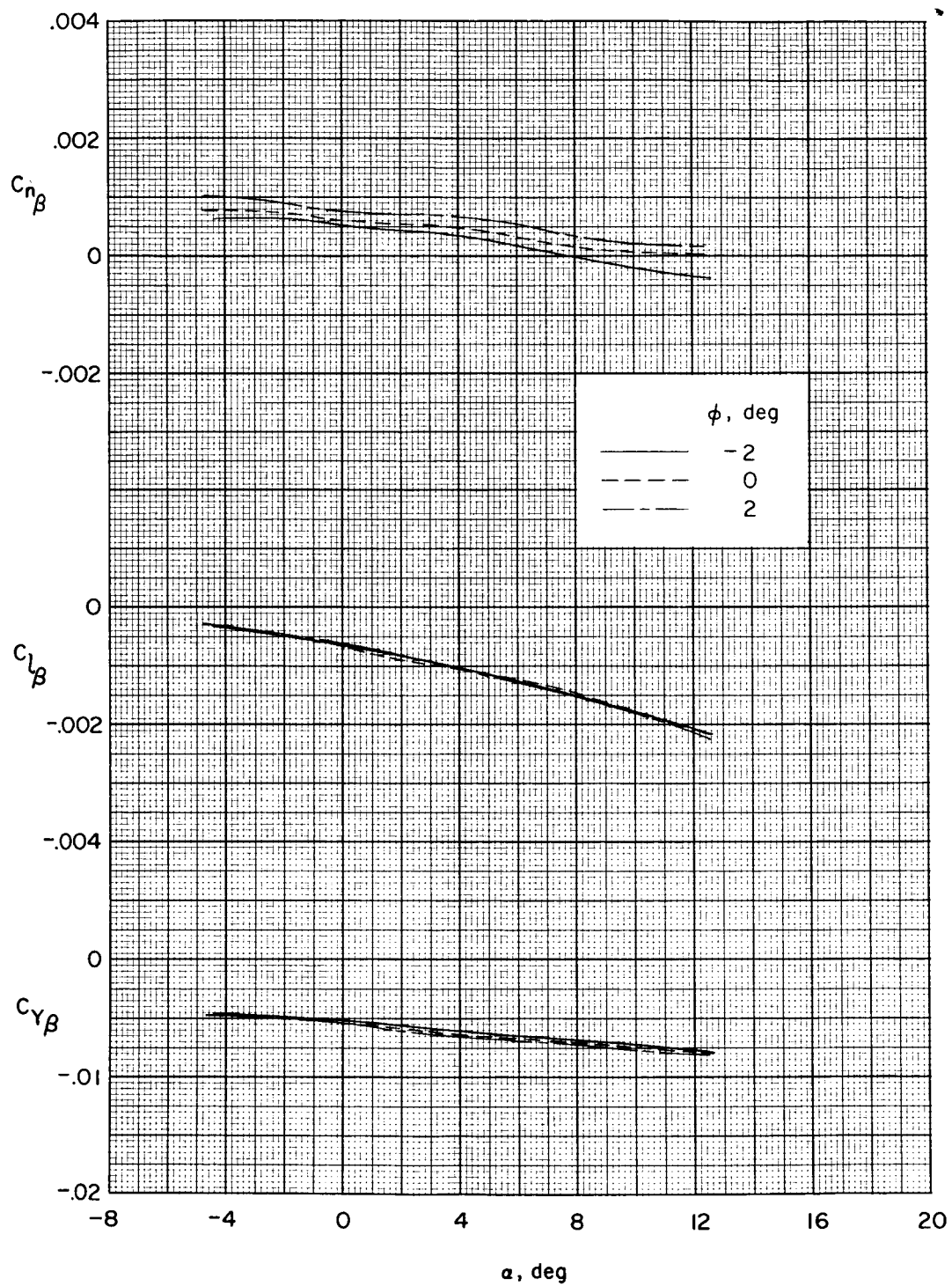
Figure 5.- Continued.





(c)  $M = 2.96$ .

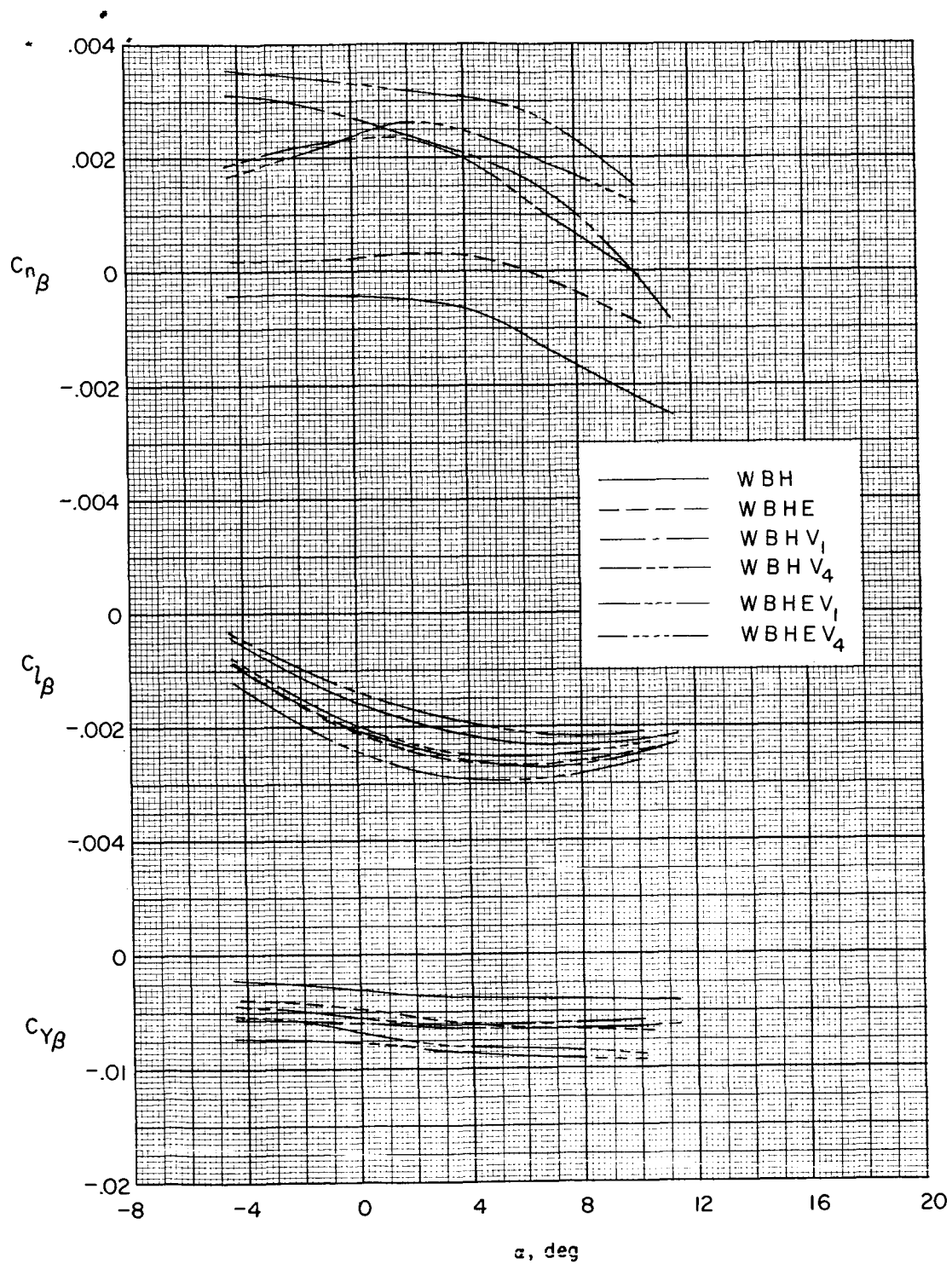
Figure 5.- Continued.



(d)  $M = 3.50$ .

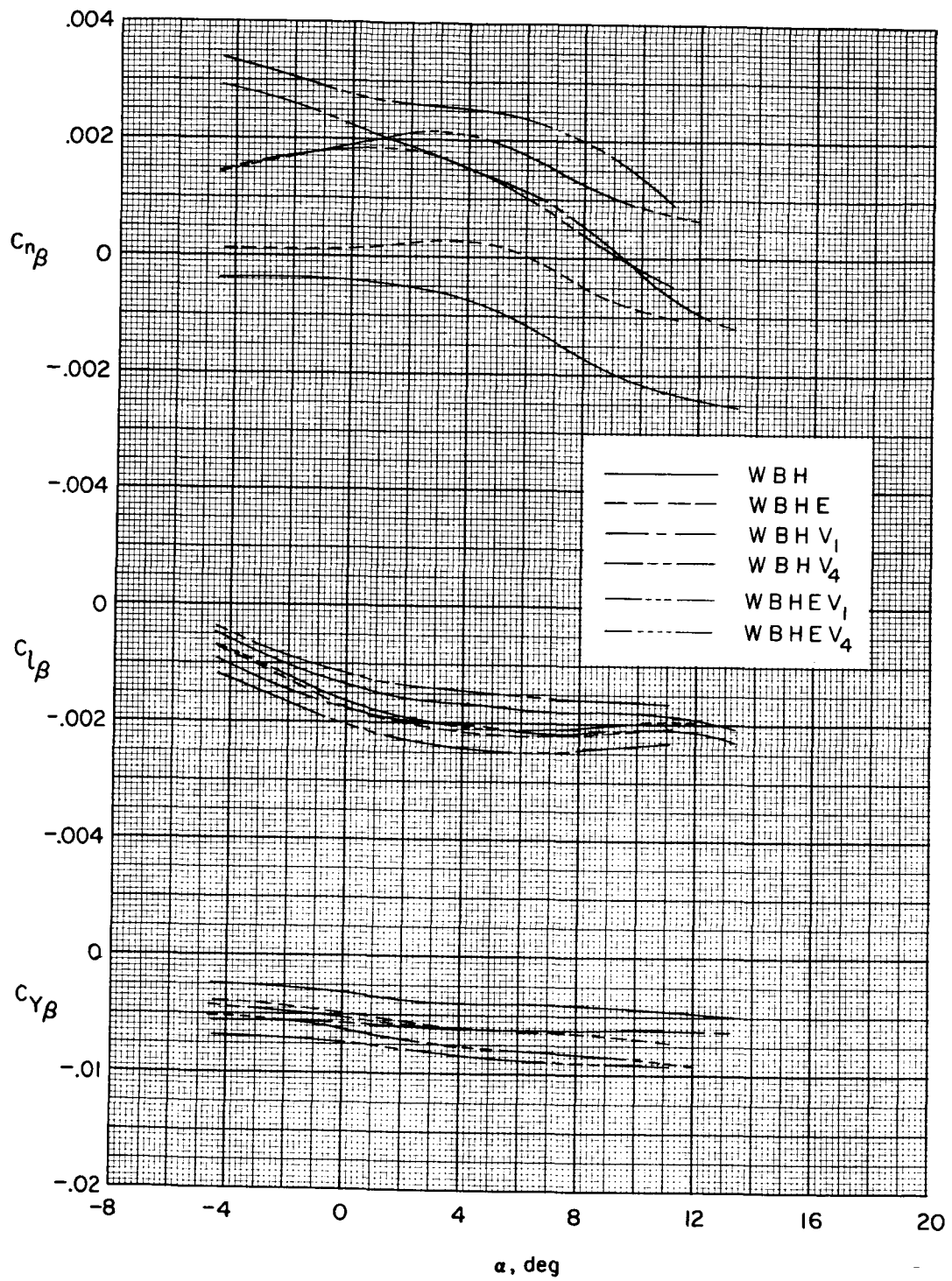
Figure 5.- Concluded.





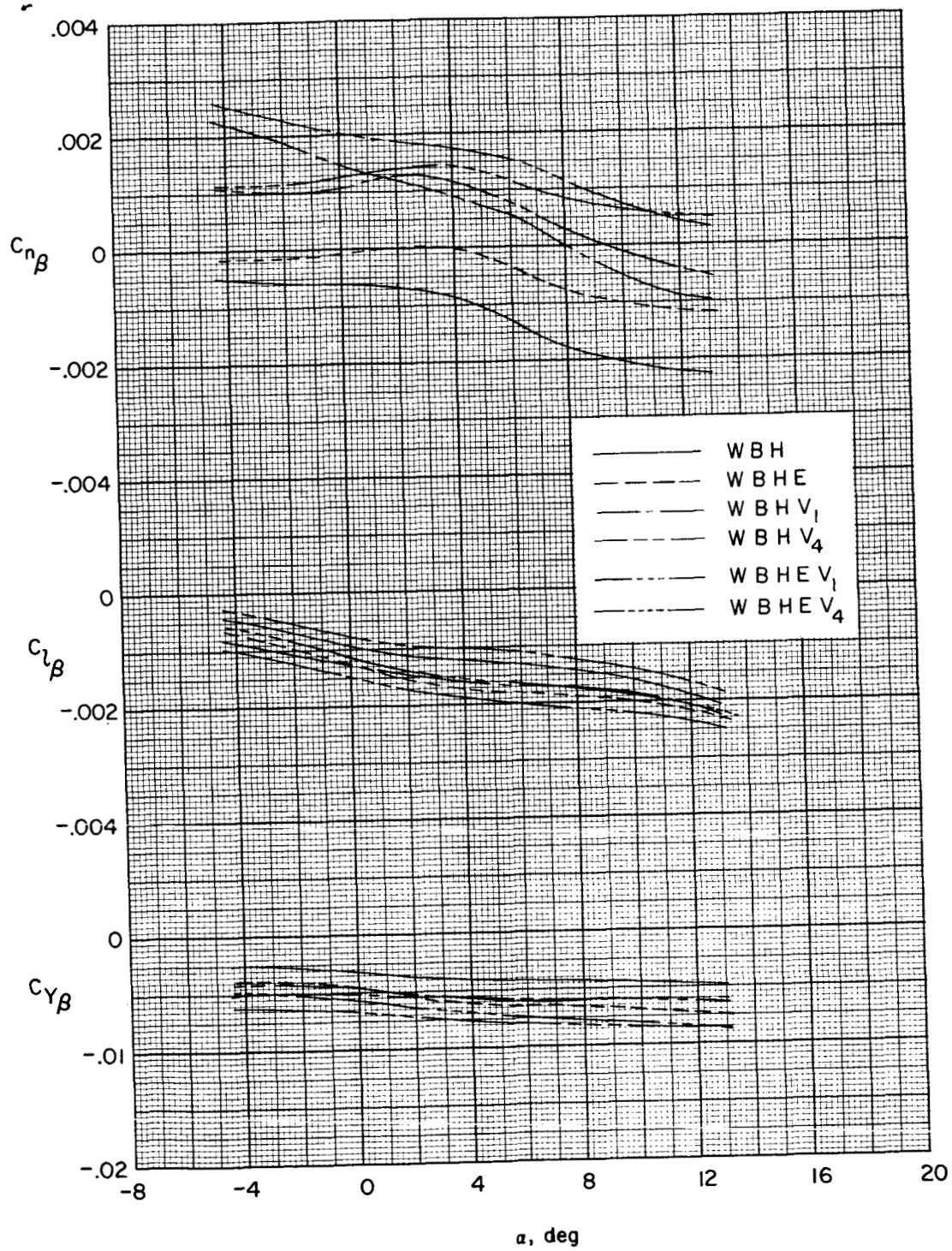
(a)  $M = 2.30$ .

Figure 6.- Effect of various components on lateral directional-stability parameters.  $\delta_h = -2^\circ$ ;  $\phi = 0^\circ$ .



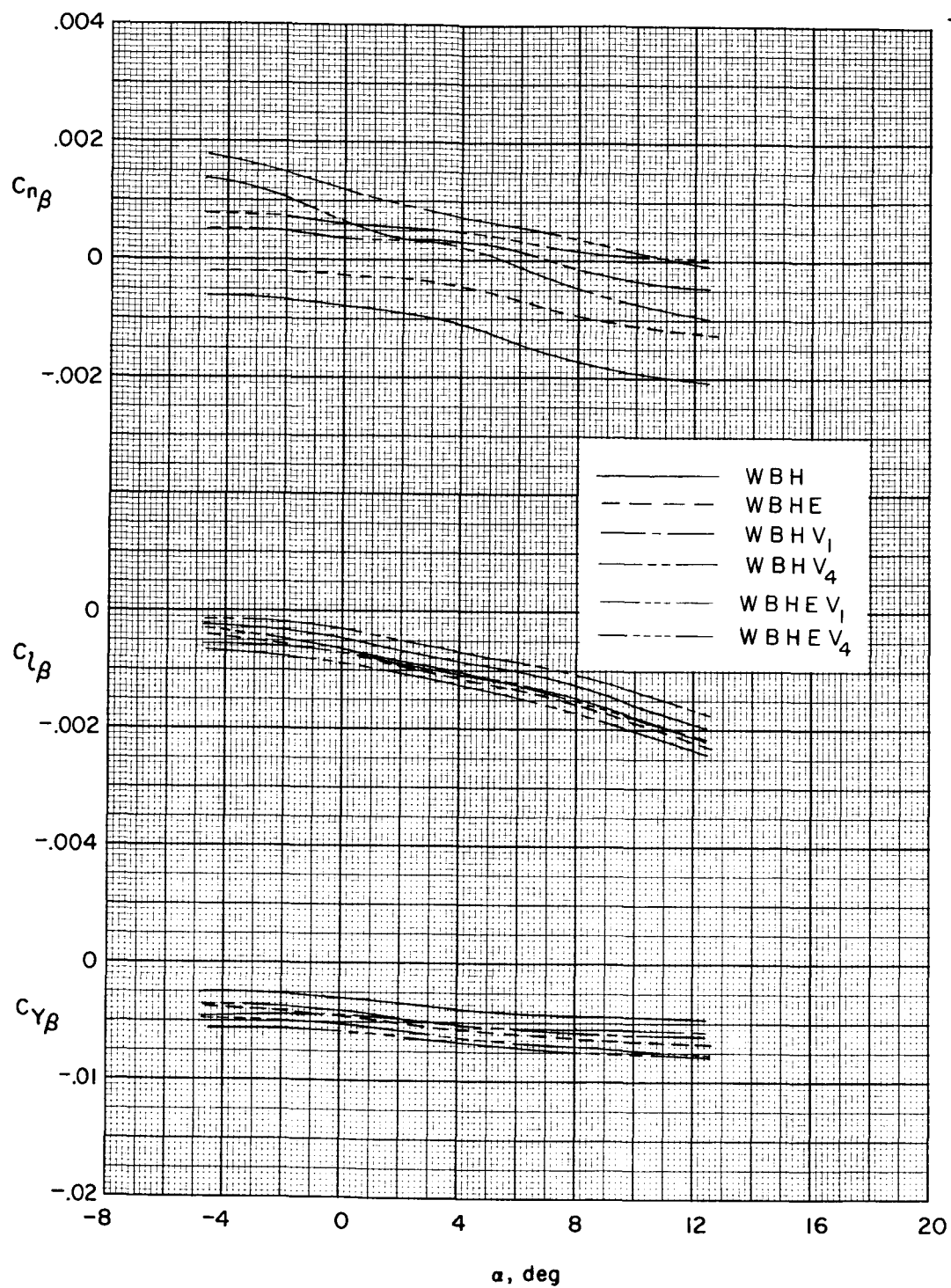
(b)  $M = 2.60$ .

Figure 6.- Continued.



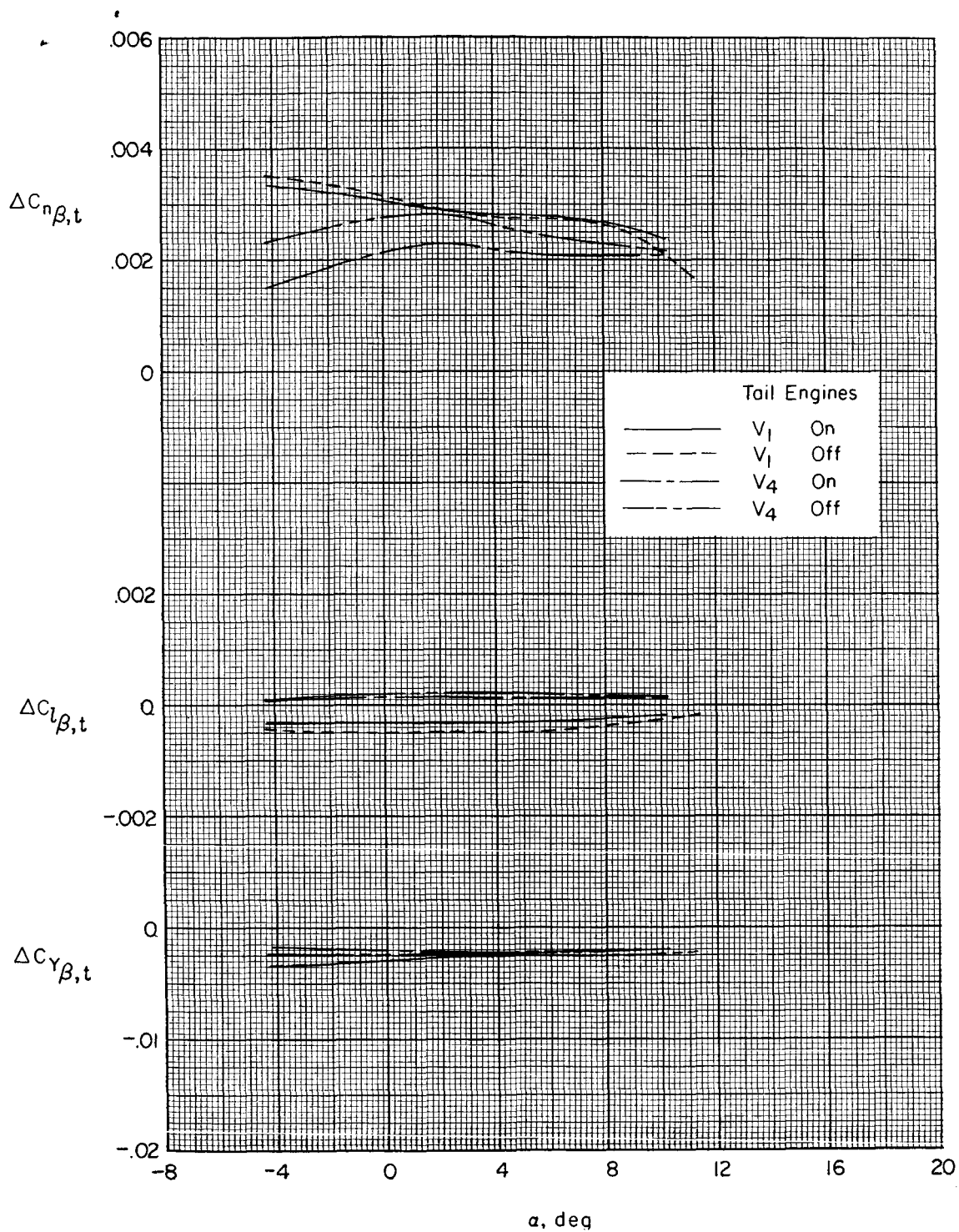
(c)  $M = 2.96$ .

Figure 6.- Continued.



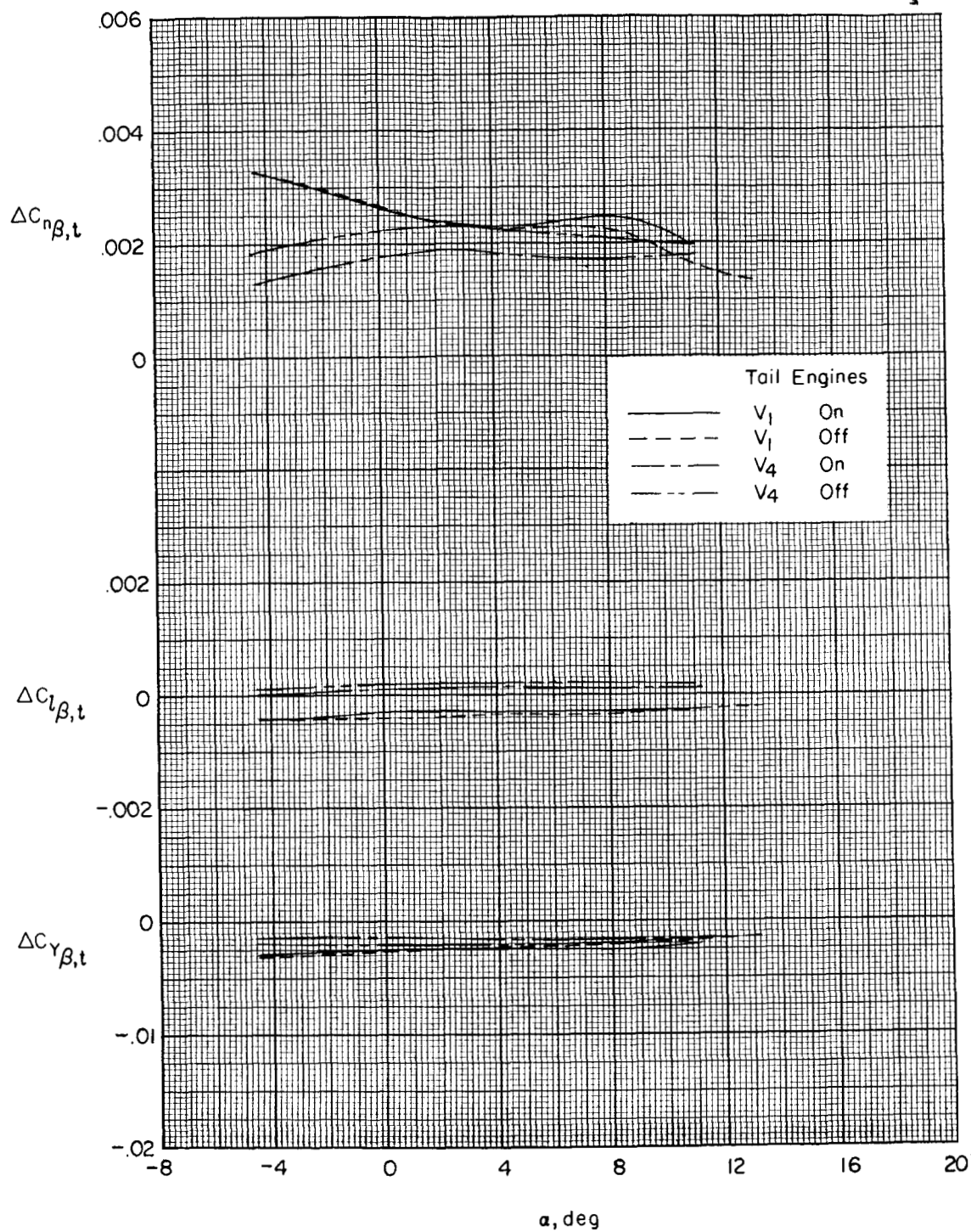
(d)  $M = 3.50$ .

Figure 6.- Concluded.



(a)  $M = 2.30$ .

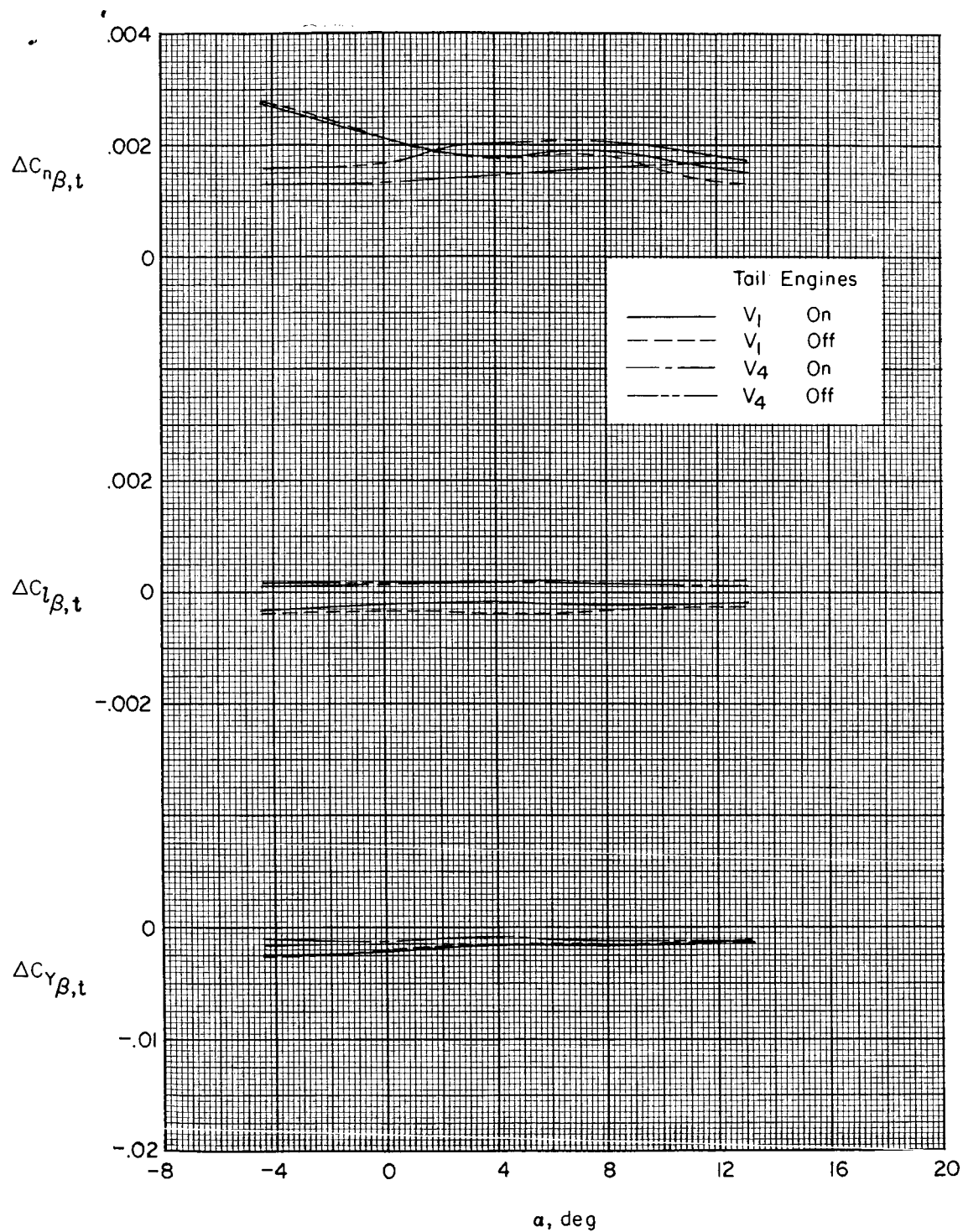
Figure 7.- Tail contributions with engine nacelles on and off.



(b)  $M = 2.60$ .

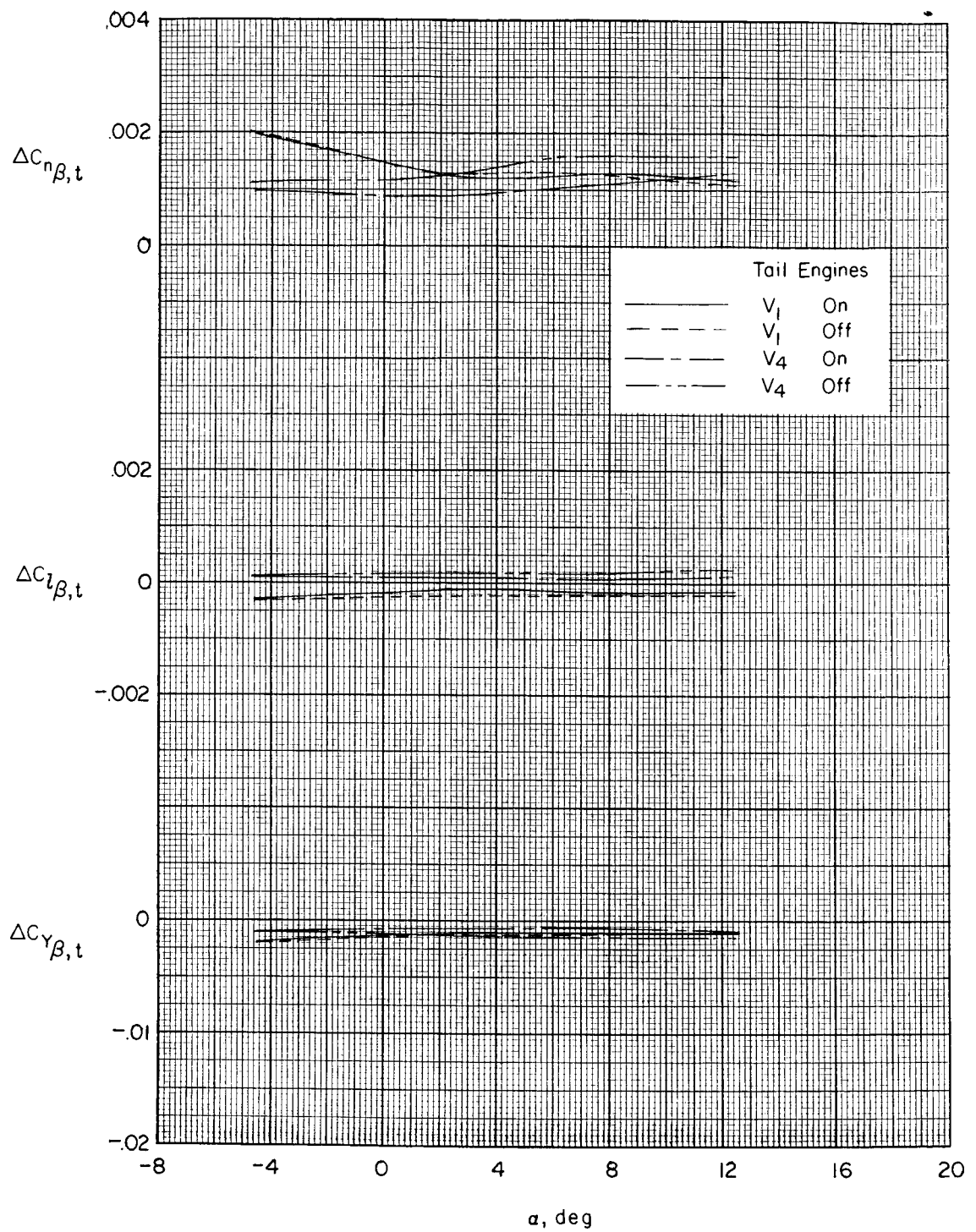
Figure 7.- Continued.





(c)  $M = 2.96$ .

Figure 7.- Continued.



(d)  $M = 3.50$ .

Figure 7.- Concluded.